

Inter-band Coulomb coupling in narrow gap semiconductor nanocrystals: $\mathbf{k} \cdot \mathbf{p}$ theory

Maryam Azizi and Paweł Machnikowski

Institute of Physics, Wrocław University of Technology, 50-370 Wrocław, Poland

(Dated: May 17, 2022)

We derive the matrix elements of Coulomb interaction between states with different number of electrons and holes in a semiconductor nanocrystal within the 8-band $\mathbf{k} \cdot \mathbf{p}$ theory. These matrix elements are responsible for multiple exciton generation which may contribute to the enhancement of the efficiency of solar cells. Our calculations are performed within the multi band envelope function formalism based on the states resulting from diagonalization of the 8-band $\mathbf{k} \cdot \mathbf{p}$ Hamiltonian. We study in detail and compare two contributions to the inter-band Coulomb coupling: the mesoscopic one, which involves only the envelope functions and relies on band mixing, and the microscopic one, that relies on the Bloch parts of the wave functions and is non-zero even between single-band states. We show that these two contributions are of a similar order of magnitude. We study also the statistical distribution of the magnitudes of the inter-band Coulomb matrix elements and show that the overall coupling to remote states decays according to a power law favorable for the convergence of numerical computations.

I. INTRODUCTION

Semiconductor nanocrystals (NCs) are of considerable current interest for exploring a large number of novel phenomena at the nanoscale and for exploiting their unique size dependent properties in potential applications. In particular, these semiconductor nanostructures have a large potential for applications in nano- and optoelectronics¹⁻⁴.

One of the interesting properties of semiconductor nanocrystals is the interband Coulomb coupling⁵⁻¹⁶ that can lead to multiple exciton generation (MEG)^{4,17,18}. In the MEG process, absorption of a single photon leads to creation of two or more electron-hole pairs, as schematically depicted in Fig. 1. This can occur when absorbing a photon is followed by creation of an electron-hole pair (an exciton) which then relaxes into an energetically lower state and the excess energy is used to create a second electron-hole pair (thus creating a biexciton state)^{7-11,19,20}. The same process can also occur coherently via a superposition of single- and bi-exciton states, or with the single exciton state playing the role of a virtual intermediate state^{13-15,21-23}. In any case, this process is mediated by Coulomb scattering between electron states in different bands which does not conserve the number of electron-hole pairs. Experiments indicate that the MEG process may indeed contribute to the efficiency of solar cells^{17,18}.

Because of its importance both for the full understanding of nanocrystal properties as well as for practical applications, the interband Coulomb couplings were extensively studied by various theoretical methods, including density functional theory^{5,6}, pseudopotential method⁷⁻¹⁰, or tight binding approach^{11,12,16,24}. Since the ab-initio and atomistic methods are computationally expensive, the less numerically demanding $\mathbf{k} \cdot \mathbf{p}$ method has also been used in the modeling of Coulomb couplings^{13,14,25-27}. This approach allows one to perform more extensive computations including coupled exciton

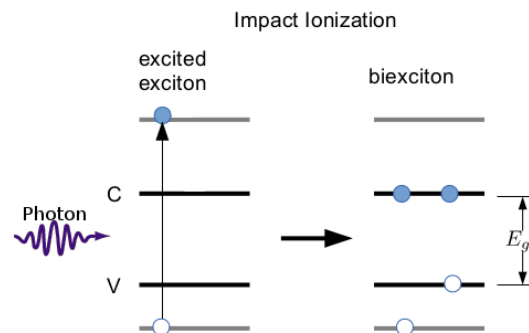


FIG. 1. (Color online) Schematic depiction of multiple exciton generation by impact ionization of a high-energy electron-hole pair.

and biexciton states in a wide energy range.

When viewed from the $\mathbf{k} \cdot \mathbf{p}$ perspective, the Coulomb coupling between few-particle states with different numbers of electron-hole pairs can appear in two ways. First, it can be due to band-mixing, with the two states coupled by the usual intraband Coulomb interaction terms involving, e.g., the conduction band admixture to a hole state²⁷. We will refer to this contribution as “mesoscopic” as the relevant matrix element involves only the envelope parts of the wave functions (similarly to the common electron-electron or electron-hole interactions computed in the usual way in a nanostructure). Second, the coupling between such configurations can appear directly when one takes the Bloch part of the wave function into account²³. This is, in turn, formally similar to the $\mathbf{k} \cdot \mathbf{p}$ calculation of electron-hole exchange coupling in a quantum dot²⁸. Because of its formal structure, we will refer to this contribution as “microscopic”. This microscopic contribution is formally reduced by a factor on the

order of a/R as compared to the mesoscopic one²³ (where a is the lattice constant and R is the nanocrystal radius) but it does not rely on band mixing (which may be a weak effect), hence it is not possible to predict *a priori* whether it will be small compared to the mesoscopic one. Estimates obtained using a simplified, single-band model of wave functions²³ yield values of this microscopic part of the matrix element up to several meV or a few tens of meV and the resulting degree of mixing between single-exciton and biexciton states is on the order of 0.1, which suggests that this contribution is not negligible.

In this paper, we present the calculations of the Coulomb matrix elements between exciton (X) and biexciton (BX) states within the multi band envelope function formalism based on the states resulting from diagonalization of the 8-band $\mathbf{k} \cdot \mathbf{p}$ Hamiltonian²⁹. Mesoscopic and microscopic contributions to the inter-band Coulomb coupling are studied in detail by generalizing the previous results²³ to the realistic model of wave functions including the band mixing. The relatively low computational cost of the $\mathbf{k} \cdot \mathbf{p}$ method allows us to find coupled pairs of X-BX states in a very broad energy window and to study the distribution of the magnitudes of the matrix elements vs. the energies of the coupled configurations in order to build reliable statistics. We show that in many cases the two contributions are of a similar order of magnitude so both need to be taken into account for reliable modeling. Moreover, we analyze the statistics of the coupling magnitudes relative to the energy distance between the two coupled states which allows us to assess the contribution of remote states to the X-BX state mixing. We confirm the findings of the simplified model²³ and show that this contribution decreases with energy distance, thus providing formal grounds for restricting numerical computations to a finite energy window.

The paper is organized as follows. In Sec. II, we define the model. In Sec. III we discuss the derivation and computation of the inter-band coulomb matrix elements. In Sec. IV, the results of our calculations are presented and discussed. Finally, Sec. V concludes the paper.

II. MODEL

In this section, we describe the model of the nanocrystal used for our calculations.

We consider a simple model of a nanostructure, defined as an InAs sphere with an infinitely high potential barrier at its boundary. The radius of the nanostructure is $R = 2.5$ nm. For the single-particle spectrum, we use the envelope function formalism with a standard 8-band Luttinger-Kohn Hamiltonian²⁹. All the material parameters relevant to the single-particle spectrum are taken from Ref. [30]. The nanocrystal is assumed to be surrounded by air. We assume the dielectric constant of InAs $\epsilon_s = 14$.

The Coulomb energy in a spherical NC is composed of the direct Coulomb interaction and the coupling via sur-

face polarization due to dielectric discontinuity between the NC and the environment. The direct part is

$$U_{\text{direct}}(\mathbf{r}, \mathbf{r}') = \frac{e^2}{4\pi\epsilon_0\epsilon_s} \frac{1}{|\mathbf{r} - \mathbf{r}'|}. \quad (1)$$

The indirect part contains the two-particle term describing mutual interaction of electrons via the polarization field,

$$U_{\text{pol}}^{(2)}(\mathbf{r}, \mathbf{r}') = -\frac{e^2}{4\pi\epsilon_0\epsilon_s} \sum_k \chi_k \frac{(rr')^k}{R^{2k+1}} P_k \left(\frac{\mathbf{r} \cdot \mathbf{r}'}{rr'} \right), \quad (2)$$

and the single particle term

$$U_{\text{pol}}^{(1)}(\mathbf{r}) = \frac{e^2}{2\epsilon_2} \sum_{n=1}^N \sum_{k=0}^{\infty} \alpha_k \frac{r^{2k}}{R^{2k+1}}, \quad (3)$$

which accounts for the self-energy contribution arising from the interaction of a charge with its own polarization field³⁰. Here P_k are Legendre polynomials and $\chi_k = (k+1)(\epsilon-1)/(k\epsilon_s+k+1)$. In addition, interaction of the electrons with the positive ‘‘jellium’’ background yields further single-particle terms.

In view of the strong quantization of the energy levels in a small nanostructure we neglect Coulomb correlations and energy shifts for the few-particle configurations and include only the inter-band Coulomb couplings that are the essence of the present study.

III. CARRIER STATES AND MATRIX ELEMENTS

In this Section, we present the systematic derivation of the interband Coulomb matrix elements (that is, matrix elements coupling single- and bi-exciton states) within the 8-band envelope function approach. First, in Sec. III A, we present the single-particle states that make up the few-particle configurations. Then, in Sec. III B, we classify all the Coulomb terms of this kind and identify those relevant to the actual exciton-biexciton coupling. Finally, in Sec. III C, we derive the matrix elements for the multi-band wave functions.

A. Single particle states

Each electron and hole state is characterized by the total angular momentum j , the projection of the total momentum $-j \leq m \leq j$, the spatial inversion parity, and an additional quantum number n labeling the subsequent wave functions with the same j , m and parity. We write the wave functions in the eight-band envelope approximation in the form

$$\Psi_{\gamma}^{\pm}(\mathbf{r}, s) = \sum_{\lambda} \varphi_{\gamma\lambda}(\mathbf{r}) u_{\lambda}(\mathbf{r}, s), \quad (4)$$

where \mathbf{r} is position, s denotes the spin projection, γ stands for the set of quantum numbers (jmn) , \pm refers the parity, $\varphi_{\gamma\lambda}(\mathbf{r})$ is the envelope function and $u_\lambda(\mathbf{r}, s)$ is lattice-periodic Bloch part. Here, λ denotes the subband within the eight-band $\mathbf{k} \cdot \mathbf{p}$ expansion: two subbands in the conduction band and six subbands in the valence band (heavy hole, light hole and spin-orbit split subbands).

In the numerical calculations, the envelope functions are further expanded into the basis functions composed of Bessel functions j_l for the radial part and spherical harmonics Y_{lm} for the angular dependence,

$$\begin{aligned} \varphi_{\gamma\lambda}(\mathbf{r}) &= \sum_{nlm} c_{nlm}^{(\gamma\lambda)} N_{nl} j_l \left(\frac{r}{R} X_{ln} \right) Y_{lm}(\theta, \varphi) \\ &\equiv \sum_{\nu} c_{\nu}^{(\gamma\lambda)} \psi_{\nu}(\mathbf{r}). \end{aligned} \quad (5)$$

Here, ν represents the three quantum numbers, nlm and $N_{nl} = \sqrt{2/|j_{l+1}(X_{ln})|}$. The summation in Eq. 5 is over $l = j \pm 1/2$ or $l = j \pm 3/2$ depending on the subband λ ²⁹. The coefficients $c_{\nu}^{(\gamma\lambda)}$ are found from numerical diagonalization of the eight-band $\mathbf{k} \cdot \mathbf{p}$ Hamiltonian²⁹ with a cut-off for n at $n_{\max} = 100$. The allowed optical transitions result from the standard dipole selection rules with their relative magnitude dependent on the overlap of the envelope functions. In particular, the optical transitions are only allowed between conduction and valence band states with the same parity.

B. Interband Coulomb coupling

In this section, we formally derive the general matrix elements between single-exciton and biexciton states (without any reference to the particular model of wave functions). We provide physical interpretation for the whole variety of these terms and indicate (on the grounds of the particular energetic relations for the case of interest) those relevant to the actual exciton-biexciton coupling.

In the ground state of a NC (to be denoted $|GS\rangle$), the valence band is fully occupied, while the conduction band is empty. Here, by valence (conduction) band we understand the single-particle eigenstates resulting from the $\mathbf{k} \cdot \mathbf{p}$ diagonalization with energies below (above) the fundamental band gap (as opposed to the original bands of a bulk crystal at $k = 0$). For the sake of more clarity in our derivations, the general index γ in the expansion Eq. 4 will be replaced by β and α for the valence and conduction band states, respectively. The corresponding

creation (annihilation) operators are $a_{\alpha}^{\dagger}(a_{\alpha})$ and $a_{\beta}^{\dagger}(a_{\beta})$ in the conduction and valence band, respectively. We denote the X and BX configurations by $|\alpha\beta\rangle = a_{\alpha}^{\dagger}a_{\beta}|GS\rangle$ and $|\alpha_1\alpha_2\beta_1\beta_2\rangle = a_{\alpha_1}^{\dagger}a_{\alpha_2}^{\dagger}a_{\beta_1}a_{\beta_2}|GS\rangle$.

The single particle terms of the Hamiltonian (that arise from electron-ion interaction and the polarization self-energy) have the form

$$H^{(1)} = \sum_{\gamma\gamma'} V_{\gamma\gamma'}^{(1)} a_{\gamma}^{\dagger} a_{\gamma'}, \quad (6)$$

where $V_{\gamma\gamma'}^{(1)} = \sum_s \int d^3r \Psi_{\gamma}^*(\mathbf{r}, s) U^{(1)}(\mathbf{r}) \Psi_{\gamma'}(\mathbf{r}, s)$. Here $U^{(1)}(\mathbf{r})$ denotes all the single particle terms in the Coulomb interaction. The only non-zero contribution to the X-BX coupling is

$$\begin{aligned} &\langle \alpha_1\alpha_2\beta_1\beta_2 | H^{(1)} | \alpha\beta \rangle \\ &= \sum_{\alpha'\beta'} V_{\alpha'\beta'}^{(1)} \langle GS | a_{\beta_2}^{\dagger} a_{\beta_1}^{\dagger} a_{\alpha_2} a_{\alpha_1} a_{\beta'}^{\dagger} a_{\alpha'} a_{\alpha}^{\dagger} a_{\beta} | GS \rangle \\ &= -V_{\alpha_1\beta_1} \delta_{\alpha_2\alpha} \delta_{\beta_2\beta} + V_{\alpha_1\beta_2} \delta_{\alpha_2\alpha} \delta_{\beta_1\beta} \\ &\quad + V_{\alpha_2\beta_1} \delta_{\alpha_1\alpha} \delta_{\beta_2\beta} - V_{\alpha_2\beta_2} \delta_{\alpha_1\alpha} \delta_{\beta_1\beta}. \end{aligned} \quad (7)$$

All these terms describe scattering processes in which a new electron-hole pair is created without changing the states of the originally existing particles. Such processes are obviously strongly off-resonant and will be disregarded.

For the two-particle terms (the two-particle part of the electron-electron interaction) the Hamiltonian can be written as

$$H^{(2)} = \frac{1}{2} \sum_{\gamma_1\gamma_2\gamma_3\gamma_4} V_{\gamma_1\gamma_2\gamma_3\gamma_4}^{(2)} a_{\gamma_1}^{\dagger} a_{\gamma_2}^{\dagger} a_{\gamma_3} a_{\gamma_4}, \quad (8)$$

where

$$\begin{aligned} V_{\gamma_1\gamma_2\gamma_3\gamma_4} &= \sum_{s,s'} \int d^3r \int d^3r' \Psi_{\gamma_1}^*(\mathbf{r}, s) \Psi_{\gamma_2}^*(\mathbf{r}', s') \\ &\quad \times U^{(2)}(\mathbf{r}, \mathbf{r}') \Psi_{\gamma_3}(\mathbf{r}', s') \Psi_{\gamma_4}(\mathbf{r}, s), \end{aligned} \quad (9)$$

and $U^{(2)}(\mathbf{r}, \mathbf{r}')$ represents all the two-particle terms of the Coulomb interaction. Hence, the matrix elements are

$$\begin{aligned} &\langle \alpha_1\alpha_2\beta_1\beta_2 | H^{(2)} | \alpha\beta \rangle = \frac{1}{2} \sum_{\gamma_1\gamma_2\gamma_3\gamma_4} V_{\gamma_1\gamma_2\gamma_3\gamma_4}^{(2)} \\ &\quad \times \langle GS | a_{\beta_2}^{\dagger} a_{\beta_1}^{\dagger} a_{\alpha_2} a_{\alpha_1} a_{\gamma_1}^{\dagger} a_{\gamma_2}^{\dagger} a_{\gamma_3} a_{\gamma_4} a_{\alpha}^{\dagger} a_{\beta} | GS \rangle. \end{aligned} \quad (10)$$

There are four assignments of the indices $\gamma_1\gamma_2\gamma_3\gamma_4$ to the valence (v) and conduction (c) bands that lead to non-zero matrix elements: (A) v cvv, (B) cv vv, (C) cv vc, and (D) cc cv.

For these assignments the matrix elements are

$$\begin{aligned}
\langle \alpha_1 \alpha_2 \beta_1 \beta_2 | H^{(2)} | \alpha \beta \rangle_A &= \langle \alpha_1 \alpha_2 \beta_1 \beta_2 | H^{(2)} | \alpha \beta \rangle_B \\
&= \frac{1}{2} \sum_{\beta'} [-V_{\beta' \alpha_1 \beta_1 \beta'} \delta_{\beta \beta_2} \delta_{\alpha \alpha_2} + V_{\beta' \alpha_2 \beta_1 \beta'} \delta_{\beta \beta_2} \delta_{\alpha \alpha_1} + V_{\beta' \alpha_1 \beta_2 \beta'} \delta_{\alpha \alpha_2} \delta_{\beta \beta_1} - V_{\beta' \alpha_2 \beta_2 \beta'} \delta_{\alpha_1 \alpha} \delta_{\beta \beta_1}] \\
&\quad + \frac{1}{2} \sum_{\beta'} [V_{\beta' \alpha_1 \beta' \beta_1} \delta_{\beta \beta_2} \delta_{\alpha \alpha_2} - V_{\beta' \alpha_1 \beta' \beta_2} \delta_{\beta \beta_1} \delta_{\alpha \alpha_2} - V_{\beta' \alpha_2 \beta' \beta_1} \delta_{\beta \beta_2} \delta_{\alpha \alpha_1} + V_{\beta' \alpha_2 \beta' \beta_2} \delta_{\beta \beta_1} \delta_{\alpha \alpha_1}] \\
&\quad + \frac{1}{2} [V_{\beta \alpha_1 \beta_1 \beta_2} \delta_{\alpha \alpha_2} - V_{\beta \alpha_2 \beta_1 \beta_2} \delta_{\alpha \alpha_1} - V_{\beta \alpha_1 \beta_2 \beta_1} \delta_{\alpha \alpha_2} + V_{\beta \alpha_2 \beta_2 \beta_1} \delta_{\alpha \alpha_1}],
\end{aligned} \tag{11}$$

and

$$\begin{aligned}
\langle \alpha_1 \alpha_2 \beta_1 \beta_2 | H^{(2)} | \alpha \beta \rangle_C &= \langle \alpha_1 \alpha_2 \beta_1 \beta_2 | H^{(2)} | \alpha \beta \rangle_D \\
&= \frac{1}{2} [-V_{\alpha_1 \alpha_2 \beta_1 \alpha} \delta_{\beta \beta_2} + V_{\alpha_2 \alpha_1 \beta_1 \alpha} \delta_{\beta \beta_2} + V_{\alpha_1 \alpha_2 \beta_2 \alpha} \delta_{\beta \beta_1} - V_{\alpha_2 \alpha_1 \beta_2 \alpha} \delta_{\beta \beta_1}],
\end{aligned} \tag{12}$$

where we used the symmetry $V_{\gamma_1 \gamma_2 \gamma_3 \gamma_4} = V_{\gamma_2 \gamma_1 \gamma_4 \gamma_3}$.

The first two lines in the contributions A and B contain the direct and exchange interactions with all the other electrons in the NC. The direct terms cancel the electron interactions in the leading order (on the mesoscopic scale). The exchange terms are not so straightforward to treat. However, all the terms containing two Kronecker deltas like $\delta_{\alpha \alpha_i} \delta_{\beta \beta_j}$, couple the two-particles state $|\alpha \beta\rangle$ to a four-particle state with two particles (electron and hole) in the same state; like $|\alpha \alpha_2, \beta \beta_2\rangle$. These two states differ considerably by energy (two particles do not change their states but a new e-h pair is created), hence these terms describe strongly off-resonant couplings and can be neglected. The last lines in the contributions A and B describe scattering processes in which one electron is a spectator, while a hole changes its state and induces generation of the second e-h pair. Since the hole energies

are typically smaller, these processes are of relatively little importance. Therefore, for the further calculations, we are left with the (identical) terms C and D that describe scattering processes in which an electron makes an intraband transition and transfer its energy to an inter-band excitation that produces another e-h pair.

C. Matrix elements

In this section we calculate the matrix elements for the explicit model of wave functions defined in Sec. III A. This is done by expressing the result in terms of standard (envelope-function) Coulomb integrals and the single-band interband matrix elements found previously²³.

The matrix elements are written as in Eq. (9)

Upon substitution of Eq. (4) in Eq. (9) one has

$$\begin{aligned}
V_{\gamma_1 \gamma_2 \gamma_3 \gamma_4} &= \sum_{\lambda_1 \lambda_2 \lambda_3 \lambda_4} \sum_{\nu_1 \nu_2 \nu_3 \nu_4} c_{\nu_1}^{*(\gamma_1 \lambda_1)} c_{\nu_2}^{*(\gamma_2 \lambda_2)} c_{\nu_3}^{(\gamma_3 \lambda_3)} c_{\nu_4}^{(\gamma_4 \lambda_4)} \sum_{\mathbf{R} \mathbf{R}'} \sum_{s s'} \int d^3 \zeta \int d^3 \zeta' \\
&\quad \times \psi_{\nu_1}^*(\mathbf{R}) u_{\lambda_1}^*(\zeta, s) \psi_{\nu_2}^*(\mathbf{R}') u_{\lambda_2}^*(\zeta', s') U^{(2)}(\mathbf{R} + \zeta, \mathbf{R}' + \zeta') \psi_{\nu_3}(\mathbf{R}') u_{\lambda_3}(\zeta', s') \psi_{\nu_4}(\mathbf{R}) u_{\lambda_4}(\zeta, s)
\end{aligned}$$

where we have followed the standard procedure of replacing the spatial integrals by summation over unit cells (\mathbf{R}) and integration over a single unit cell (ζ). In view of orthogonality of Bloch functions,

$$\sum_s \int d^3 \zeta u_{\lambda}^*(\zeta, s) u_{\lambda'}(\zeta, s) = \delta_{\lambda \lambda'} v,$$

where, v is the volume of the unit cell, two essentially different cases appear depending on the bands involved. If $\lambda_1 = \lambda_4$ and $\lambda_2 = \lambda_3$ then, in the leading order, one can set $U^{(2)}(\mathbf{R} + \zeta, \mathbf{R}' + \zeta') = U^{(2)}(\mathbf{R}, \mathbf{R}')$. The corresponding contribution to the matrix element is

$$\begin{aligned}
V_{\gamma_1 \gamma_2 \gamma_3 \gamma_4}^{(0)} &= \sum_{\lambda_1 \lambda_2} \sum_{\nu_1 \nu_2 \nu_3 \nu_4} c_{\nu_1}^{*(\gamma_1 \lambda_1)} c_{\nu_2}^{*(\gamma_2 \lambda_2)} c_{\nu_3}^{(\gamma_3 \lambda_2)} c_{\nu_4}^{(\gamma_4 \lambda_1)} \sum_{\mathbf{R} \mathbf{R}'} \psi_{\nu_1}^*(\mathbf{R}) \psi_{\nu_2}^*(\mathbf{R}') U^{(2)}(\mathbf{R}, \mathbf{R}') \psi_{\nu_3}(\mathbf{R}') \psi_{\nu_4}(\mathbf{R}) \\
&\quad \times \sum_s \int d^3 \zeta u_{\lambda_1}^*(\zeta, s) u_{\lambda_1}(\zeta, s) \sum_{s'} \int d^3 \zeta' u_{\lambda_2}^*(\zeta', s') u_{\lambda_2}(\zeta', s').
\end{aligned}$$

Using Eq. (13), and returning to integration according to $v \sum_{\mathbf{R}} \rightarrow \int d^3 R$, one finds

$$V_{\gamma_1 \gamma_2 \gamma_3 \gamma_4}^{(0)} = \sum_{\lambda_1 \lambda_2} \sum_{\nu_1 \nu_2 \nu_3 \nu_4} c_{\nu_1}^{*(\gamma_1 \lambda_1)} c_{\nu_2}^{*(\gamma_2 \lambda_2)} c_{\nu_3}^{(\gamma_3 \lambda_2)} c_{\nu_4}^{(\gamma_4 \lambda_1)} h_{\nu_1 \nu_2 \nu_3 \nu_4}^{(0)}$$

where

$$h_{\nu_1 \nu_2 \nu_3 \nu_4}^{(0)} = \int d^3 R \int d^3 R' \psi_{\nu_1}^*(\mathbf{R}) \psi_{\nu_2}^*(\mathbf{R}') U^{(2)}(\mathbf{R}, \mathbf{R}') \psi_{\nu_3}(\mathbf{R}') \psi_{\nu_4}(\mathbf{R}). \quad (13)$$

If $\lambda_1 = \lambda_4$ but $\lambda_2 \neq \lambda_3$ then the previously calculated contribution vanishes due to orthogonality of Bloch functions. In this case, we expand

$$U^{(2)}(\mathbf{R} + \boldsymbol{\zeta}, \mathbf{R}' + \boldsymbol{\zeta}') \approx U^{(2)}(\mathbf{R}, \mathbf{R}') + \nabla_{\mathbf{R}'} U^{(2)}(\mathbf{R}, \mathbf{R}') \cdot \boldsymbol{\zeta}'.$$

The corresponding contribution to the matrix element is then

$$\begin{aligned} V_{\gamma_1 \gamma_2 \gamma_3 \gamma_4}^{(1a)} &= \sum_{\lambda_1 \lambda_2 \lambda_3} \sum_{\nu_1 \nu_2 \nu_3 \nu_4} c_{\nu_1}^{*(\gamma_1 \lambda_1)} c_{\nu_2}^{*(\gamma_2 \lambda_2)} c_{\nu_3}^{(\gamma_3 \lambda_3)} c_{\nu_4}^{(\gamma_4 \lambda_1)} \sum_{\mathbf{R} \mathbf{R}'} \psi_{\nu_1}^*(\mathbf{R}) \psi_{\nu_2}^*(\mathbf{R}') \nabla_{\mathbf{R}'} U^{(2)}(\mathbf{R}, \mathbf{R}') \psi_{\nu_3}(\mathbf{R}') \psi_{\nu_4}(\mathbf{R}) \\ &\cdot \sum_s \int d^3 \zeta u_{\lambda_1}^*(\boldsymbol{\zeta}, s) u_{\lambda_1}(\boldsymbol{\zeta}, s) \sum_{s'} \int d^3 \zeta' u_{\lambda_2}^*(\boldsymbol{\zeta}', s') \zeta' u_{\lambda_3}(\boldsymbol{\zeta}', s') \\ &= \sum_{\lambda_1 \lambda_2 \lambda_3} \sum_{\nu_1 \nu_2 \nu_3 \nu_4} c_{\nu_1}^{*(\gamma_1 \lambda_1)} c_{\nu_2}^{*(\gamma_2 \lambda_2)} c_{\nu_3}^{(\gamma_3 \lambda_3)} c_{\nu_4}^{(\gamma_4 \lambda_1)} h_{\nu_1 \nu_2 \nu_3 \nu_4}^{(\lambda_1 \lambda_2 \lambda_3 \lambda_1)}, \end{aligned}$$

where, replacing summation over unit cells by integration as previously,

$$\begin{aligned} h_{\nu_1 \nu_2 \nu_3 \nu_4}^{(\lambda_1 \lambda_2 \lambda_3 \lambda_1)} &= \int d^3 R \int d^3 R' \\ &\times \psi_{\nu_1}^*(\mathbf{R}) \psi_{\nu_2}^*(\mathbf{R}') \mathbf{r}_{\lambda_2 \lambda_3} \cdot \nabla_{\mathbf{R}'} U^{(2)}(\mathbf{R}, \mathbf{R}') \psi_{\nu_3}(\mathbf{R}') \psi_{\nu_4}(\mathbf{R}) \end{aligned} \quad (14)$$

and

$$\mathbf{r}_{\lambda_2 \lambda_3} = \frac{1}{V} \sum_s \int d^3 \zeta' u_{\lambda_2}^*(\boldsymbol{\zeta}', s') \zeta' u_{\lambda_3}(\boldsymbol{\zeta}', s').$$

In a similar way, if $\lambda_2 = \lambda_3$ and $\lambda_1 \neq \lambda_4$ then

$$\begin{aligned} V_{\gamma_1 \gamma_2 \gamma_3 \gamma_4}^{(1b)} &= \sum_{\lambda_1 \lambda_2 \lambda_4} \sum_{\nu_1 \nu_2 \nu_3 \nu_4} c_{\nu_1}^{*(\gamma_1 \lambda_1)} c_{\nu_2}^{*(\gamma_2 \lambda_2)} c_{\nu_3}^{(\gamma_3 \lambda_2)} c_{\nu_4}^{(\gamma_4 \lambda_4)} h_{\nu_1 \nu_2 \nu_3 \nu_4}^{(\lambda_1 \lambda_2 \lambda_2 \lambda_4)}, \end{aligned}$$

where

$$h_{\nu_1 \nu_2 \nu_3 \nu_4}^{(\lambda_1 \lambda_2 \lambda_2 \lambda_4)} = h_{\nu_2 \nu_1 \nu_4 \nu_3}^{(\lambda_2 \lambda_1 \lambda_1 \lambda_3)}. \quad (15)$$

The terms with $\lambda_1 \neq \lambda_4$ and $\lambda_2 \neq \lambda_3$ contribute only in the second order in the expansion of the Coulomb potential, hence are formally on the order of $(a/R)^2$ and will not be considered here. Thus, finally, one finds

$$\begin{aligned} V_{\gamma_1 \gamma_2 \gamma_3 \gamma_4} &= \sum_{\lambda_1 \lambda_2 \lambda_3 \lambda_4} \sum_{\nu_1 \nu_2 \nu_3 \nu_4} c_{\nu_1}^{*(\gamma_1 \lambda_1)} c_{\nu_2}^{*(\gamma_2 \lambda_2)} c_{\nu_3}^{(\gamma_3 \lambda_3)} c_{\nu_4}^{(\gamma_4 \lambda_4)} \\ &\times \begin{cases} h_{\nu_1 \nu_2 \nu_3 \nu_4}^{(0)} & \text{if } \lambda_1 = \lambda_4 \text{ and } \lambda_2 = \lambda_3, \\ h_{\nu_1 \nu_2 \nu_3 \nu_4}^{(\lambda_1 \lambda_2 \lambda_3 \lambda_1)} & \text{if } \lambda_1 = \lambda_4 \text{ and } \lambda_2 \neq \lambda_3, \\ h_{\nu_2 \nu_1 \nu_4 \nu_3}^{(\lambda_2 \lambda_1 \lambda_4 \lambda_2)} & \text{if } \lambda_1 \neq \lambda_4 \text{ and } \lambda_2 = \lambda_3, \\ 0 & \text{if } \lambda_1 \neq \lambda_4 \text{ and } \lambda_2 \neq \lambda_3, \end{cases} \end{aligned}$$

which includes terms up to the first order in the expansion of the Coulomb potential. In this way, we have reduced the calculation of inter-band Coulomb matrix elements between X and BX states with 8-band wave functions to single-subband terms given by Eq. (13) and Eq. (15). The former only involve the envelope functions that describe the carrier states on the mesoscopic level and can be calculated in a standard way. The latter depend on the microscopic, atomic-scale structure via the interband matrix element of the position vector $\mathbf{r}_{\lambda \lambda'}$, which is proportional to the inter-band dipole moment (involved in the optical selection rules). These microscopic terms for the basis states used here have been calculated in Ref. [23]. Note that in the single-band approximation, when the states above and below the gap are assumed to be composed purely of the bulk conduction and valence band states, respectively, the mesoscopic term vanishes due to Bloch function orthogonality. In general, due to band mixing in a strongly confining nanostructure, both the mesoscopic and microscopic contributions can be non-zero.

IV. RESULTS

In this section, we present results of calculations performed within the eight-band model presented above. We focus on the comparison between the typical magnitudes of the microscopic and mesoscopic contributions of the inter-band Coulomb couplings and on the general statistical distribution of the coupling strengths between optically active (bright) X states and BX states vs. the energy difference between the two coupled states. In

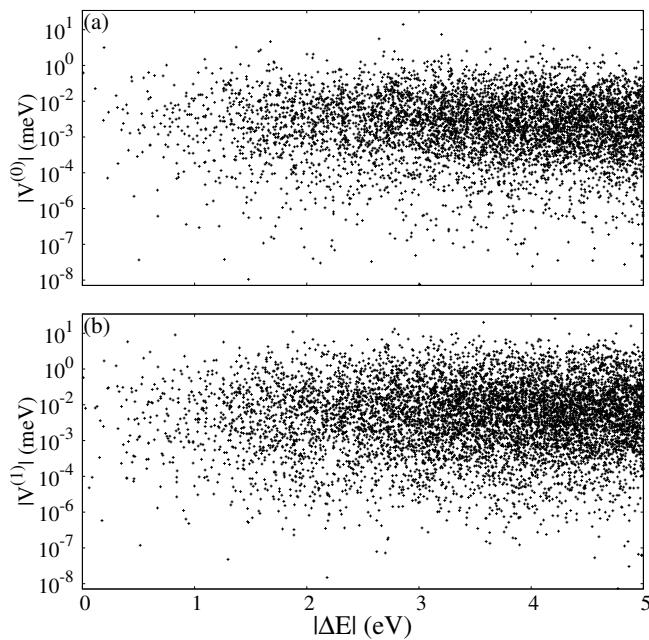


FIG. 2. The absolute value of the mesoscopic (a) and microscopic (b) contributions to the Coulomb coupling matrix elements between X and BX states vs. the energy distance between these states for a sample of 11 000 coupled X-BX pairs.

view of the enormous number of exciton and, in particular, biexciton states, the statistics of interband Coulomb couplings to be presented here are obtained by randomly selecting states from a broad energy range (using a uniform distribution over the set of quantum numbers).

In order to characterize the typical X-BX Coulomb coupling strengths and the distribution of the relative energies of coupled X-BX pairs, in Fig. 2 we present the magnitudes of these couplings vs. the energy distance between the coupled states. The presented results are based on about 50 000 randomly selected combinations of X and BX states with the energy less than 5 eV out of which 11 000 show non-zero coupling, which is still only a tiny fraction of the total number of possible X-BX combinations. Each point corresponds to a single BX state coupled to an X state and its position shows the magnitude of the Coulomb matrix element between these two states and the absolute value of the energy difference between these states. The analysis is performed separately for the mesoscopic and microscopic contributions to the Coulomb matrix elements, $V^{(0)}$ and $V^{(1)}$, shown in Fig. 2(a) and Fig. 2(b), respectively. As can be seen in Fig. 2, the overall number of coupled pairs grows with increasing energy difference. This is due to rapid increase of the density of states of both X and BX states at higher energies. Typical orders of magnitude for the X-BX coupling are up to several meV. Although we have found a small number of stronger couplings, about

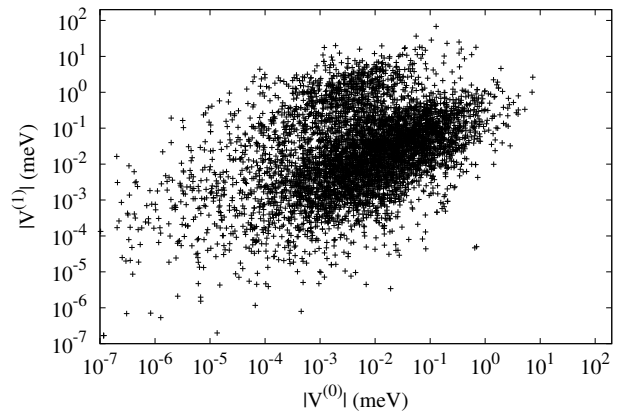


FIG. 3. Comparison of the magnitudes of micro- and mesoscopic contributions to the interband Coulomb coupling. Each point corresponds to one coupled X – BX pair from a sample of 11 000 and its position represents the magnitudes of the two contributions to the coupling.

100 meV, they only appear between energetically very distant states. Apart from this upper bound on the magnitudes of the matrix elements, Fig. 2 indicates that matrix elements with values below 10^{-6} meV are unusual, which agrees with the earlier atomistic results for another material system²⁴.

From Fig. 2 it is clear that the microscopic and mesoscopic contributions to the Coulomb coupling tend to be roughly of the same order of magnitude. This is confirmed in Fig. 3, where the magnitudes of the contributions to the Coulomb coupling for the same number of the combinations as in Fig. 2 are compared. In vast majority of coupled X-BX configurations both contributions are non-zero, which results from identical selection rules for these two couplings (the fractions of cases with only $V^{(0)}$ or only $V^{(1)}$ non-zero are about 0.2% and 4%, respectively). As we can see, although the ratio of the two contributions in individual cases can vary over 10 orders of magnitude (roughly from 10^{-5} to 10^5), in most cases they are almost of the same order of magnitude.

The same property can be seen when one looks at the histogram showing the number of state combinations as a function of $\log |V^{(1)}/V^{(0)}|$ (Fig. 4). Here we used a larger sample of 200 000 X-BX pairs out of which over 40 000 were coupled. The bimodal form of the distribution reflects the two groups of points visible in Fig. 4, corresponding to the cases where the two contributions are of similar magnitude and those where the microscopic contribution dominates by about two orders of magnitude. The origin of this special distribution remains unclear.

As discussed in Ref. [23], the distribution of the ratio of the coupling magnitude $V = V^{(0)} + V^{(1)}$ to the energy separation between the coupled states ΔE is of major importance for the convergence of numerical procedures: Since $q = |V/\Delta E|$ determines (via perturbation theory) the admixture of a biexciton state to the opti-

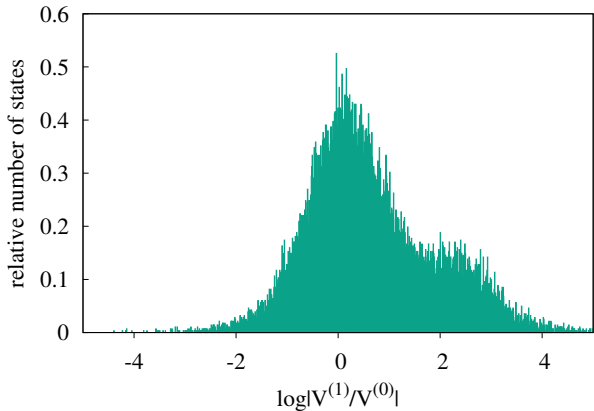


FIG. 4. Normalized distribution of the relative magnitudes of the micro- and mesoscopic couplings based on a sample of about 40 000 coupled X-BX pairs.

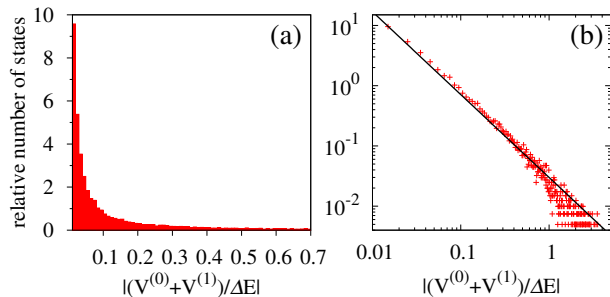


FIG. 5. Histogram of the values of the ratio $q = |(V^{(0)} + V^{(1)})/\Delta E|$ for a sample of about 40 000 coupled X-BX pairs in linear (a) and logarithmic (b) scale. The solid line in (b) shows a q^{-2} dependence.

cally active single-exciton state, the distribution of this quantity must be integrable at $q \rightarrow 0$ in order for the computations to be convergent with respect to the width of the energy window in which the states have been found (which is always limited by the available computational resources). Statistics based on a simplistic model of carrier states yielded a q^{-2} dependence as $q \rightarrow 0$, which pro-

vides a bound for the contribution of remote states (in view of the bounded values of the coupling magnitudes) and thus assures convergence²³. The results presented in Fig. 5 (based on the sample as in Fig. 4) confirm that the same q^{-2} form of the distribution is found in the present, more realistic model, as shown by the solid line in Fig. 5(b).

V. CONCLUSIONS

We have presented a method for calculating Coulomb matrix elements between exciton and biexciton states in a spherical semiconductor nanoparticle within the multi-band envelope function formalism based on the carrier states resulting from diagonalization of the 8-band $\mathbf{k} \cdot \mathbf{p}$ Hamiltonian. We have shown that this coupling includes two contributions of different form: The mesoscopic one relies on the usual inter-band Coulomb matrix elements that contribute to inter-band couplings via band mixing. The microscopic contribution involves Coulomb matrix elements at the level of Bloch functions and does not vanish even if band mixing is neglected.

The relatively low computational cost of the $\mathbf{k} \cdot \mathbf{p}$ method allowed us to build statistics of the coupling values over $\sim 10^5$ X-BX pairs in a broad energy window relevant, e.g., to photoelectric cell operation. We have shown that the relative magnitude of these two contributions over a large statistical sample of X-BX pairs has a bimodal distribution with either both contributions equal or the microscopic one dominating roughly by two orders of magnitude.

We have also shown within our multi-band model that the ratio of the coupling magnitude to the energy separation between the coupled states follows a power-law distribution the exponent of which guarantees convergence of numerical calculations with respect to the width of the energy window to which such a computation must always be limited.

Acknowledgments

This work was supported by the TEAM programme of the Foundation for Polish Science co-financed from the European Regional Development Fund.

¹ D. V. Talapin, J.-S. Lee, M. V. Kovalenko, and E. V. Shevchenko, *Chem. Rev.* **110**, 389 (2010).

² T. V. Teperik and A. Degiron, *Phys. Rev. Lett.* **108**, 147401 (2012).

³ L. Peng, L. Hu, and X. Fang, *Advanced Materials* **25**, 5321 (2013).

⁴ D. J. Binks, *Phys. Chem. Chem. Phys.* **13**, 12693 (2011).

⁵ K. Hyeon-Deuk and O. V. Prezhdo, *Nano Lett.* **11**, 1845 (2011).

⁶ K. Hyeon-Deuk and O. V. Prezhdo, *ACS Nano* **6**, 1239

(2012).

⁷ A. Franceschetti, J. M. An, and A. Zunger, *Nano Lett.* **6**, 2191 (2006).

⁸ E. Rabani and R. Baer, *Nano Lett.* **8**, 4488 (2008).

⁹ M. Califano, *ACS Nano* **3**, 2706 (2009).

¹⁰ R. Baer and E. Rabani, *Nano Lett.* **12**, 2123 (2012).

¹¹ G. Allan and C. Delerue, *Phys. Rev. B* **73**, 205423 (2006).

¹² C. Delerue, G. Allan, J. J. H. Pijpers, and M. Bonn, *Phys. Rev. B* **81**, 125306 (2010).

¹³ A. Shabaev, A. L. Efros, and A. J. Nozik, *Nano Lett.* **6**,

- 2856 (2006).
- ¹⁴ W. M. Witzel, A. Shabaev, C. S. Hellberg, V. L. Jacobs, and A. L. Efros, *Phys. Rev. Lett.* **105**, 137401 (2010).
- ¹⁵ L. Silvestri and V. M. Agranovich, *Phys. Rev. B* **81**, 205302 (2010).
- ¹⁶ M. Korkusinski, O. Voznyy, and P. Hawrylak, *Phys. Rev. B* **82**, 245304 (2010).
- ¹⁷ J. B. Sambur, T. Novet, and B. A. Parkinson, *Science* **330**, 63 (2010).
- ¹⁸ O. E. Semonin, J. M. Luther, S. Choi, H.-Y. Chen, J. Gao, A. J. Nozik, and M. C. Beard, *Science* **334**, 1530 (2011).
- ¹⁹ F. Schulze, M. Schoth, U. Woggon, A. Knorr, and C. Weber, *Phys. Rev. B* **84**, 125318 (2011).
- ²⁰ M. Azizi and P. Machnikowski, *Phys. Rev. B* **88**, 115303 (2013).
- ²¹ R. D. Schaller, V. M. Agranovich, and V. I. Klimov, *Nat. Phys.* **1**, 189 (2005).
- ²² V. I. Rupasov and V. I. Klimov, *Phys. Rev. B* **76**, 125321 (2007).
- ²³ P. Kowalski, L. Marcinowski, and P. Machnikowski, *Phys. Rev. B* **87**, 075309 (2013).
- ²⁴ M. Korkusinski, O. Voznyy, and P. Hawrylak, *Phys. Rev. B* **84**, 155327 (2011).
- ²⁵ L. Silvestri and V. M. Agranovich, *Phys. Rev. B* **81**, 205302 (2010).
- ²⁶ A. Piryatinski and K. A. Velizhanin, *J. Chem. Phys.* **133**, 084508 (2010).
- ²⁷ K. A. Velizhanin and A. Piryatinski, *Phys. Rev. Lett.* **106**, 207401 (2011).
- ²⁸ E. Kadantsev and P. Hawrylak, *Phys. Rev. B* **81**, 045311 (2010).
- ²⁹ A. L. Efros and M. Rosen, *Phys. Rev. B* **58**, 7120 (1998).
- ³⁰ L. E. Brus, *J. Chem. Phys.* **80**, 4403 (1984).